PCCP

Accepted Manuscript

This is an *Accepted Manuscript*, which has been through the Royal Society of Chemistry peer review process and has been accepted for publication.

Accepted Manuscripts are published online shortly after acceptance, before technical editing, formatting and proof reading. Using this free service, authors can make their results available to the community, in citable form, before we publish the edited article. We will replace this *Accepted Manuscript* with the edited and formatted *Advance Article* as soon as it is available.

You can find more information about *Accepted Manuscripts* in the Information for Authors.

Please note that technical editing may introduce minor changes to the text and/or graphics, which may alter content. The journal's standard Terms & Conditions and the Ethical guidelines still apply. In no event shall the Royal Society of Chemistry be held responsible for any errors or omissions in this *Accepted Manuscript* or any consequences arising from the use of any information it contains.

ROYAL SOCIETY
OF **CHEMISTRY**

www.rsc.org/pccp

Bipolar Doping of Double-layer Graphene Vertical Heterostructures with Hydrogenated Boron Nitride†

Zhun Liu[1], Ru-Zhi Wang[1, 2,*], Li-Min Liu[2, *], Woon-Ming Lau[2] and Hui Yan[1]

1）College of Materials Science and Engineering, Beijing University of Technology, Beijing 100124, China

2) Beijing Computational Science Research Centre, Beijing, 100084, China

Abstract

Using first-principles calculations, we examined the bipolar doping of double-layer graphene vertical heterostructures, which are constructed by hydrogenated boron nitride (BN) sheets sandwiched into two parallel graphene monolayers. The built-in potential difference in hydrogenated BN breaks the interlayer symmetry, resulting in the p- and n-type doping of two graphene layers by 0.83 and -0.8 eV, respectively. By tuning the interlayer spacing between the graphene and hydrogenated BN, the interfacial dipole and screening charge distribution can be affected significantly, which produces large modulations in band alignments, doping levels and tunnel barriers. Furthermore, we present an analytical model to predicate the doping level as a function of the average interlayer spacing. With large interlayer spacings, the "pillow effect" (Pauli repulsion at the highly charge overlapped interface) are diminished and the calculated Dirac point shifts are in good accordance with our prediction models. Our investigations suggest that this double-layer graphene heterostructures constructed by two-dimensional Janus anisotropic materials offer

---

*To whom correspondence should be addressed: wrz@bjut.edu.cn; limin.liu@csrc.ac.cn

Physical Chemistry Chemical Physics Accepted Manuscript

exciting opportunities for developing novel nanoscale optoelectronic and electronic devices.

Keywords: Vertical heterostructures, Hydrogenated boron nitride, Double-layer graphene, Polarization, Bipolar doping

Physical Chemistry Chemical Physics Accepted Manuscript

I. Introduction

Graphene has recently emerged as both fundamental research and novel technologically device due to its unusual electric and physical properties, such as the giant carrier mobility,[1, 2] Klein tunneling and Veselago lensing,[3] thereby enabling promising application including photodetectors, transistors, and biosensors.[1-5] Due to its zero band gap semimetal property and unimpeded electron transport through in-plane p-n junctions, lateral graphene heterostructures have limited ON-OFF switching ratios, thereby hindering their application in logic switching and integrated circuits.[1, 2, 6] An alternative solution to overcome the above issue is to use double layer graphene (DLG) vertical heterostructures, which is made of a thin insulating tunnel barrier (h-BN) sandwiched in two closely-spaced monolayer graphene.[7, 8] Recent experiment studies have demonstrated that the DLG field effect tunneling transistor exhibits even 10 times higher ON-OFF ratios than the planar graphene one.[8, 9] Owing to the low density of states near the Dirac point, DLG vertical heterostructures can be doped by gate voltages to achieve the desired carrier concentration and tunnel barrier.[3, 8, 10-12]

Similar strategies, including multiple electrostatic gating, spatially selective chemical doping treatment, asymmetric metal electrodes, and van der Waals (vdW) heterostructures, were applied to built-in potential difference for vertical graphene heterostructures.[5, 11, 13-15] However, these approaches also have different drawbacks, such as high gate voltage, costly local gating technique, inhomogeneous dopant distribution, and unusual interlayer recombination, which greatly hinder the practical application of vertical graphene as ultrafast photodetectors.[5, 13-16] Importantly, if a source-drain bias voltage is applied to separate the electron-hole pairs in photoexcited graphene, a large dark current is generated, resulting in a significant shot noise in photocurrent.[1, 17] Therefore, it is legitimate to motivate study how bipolar doping the DLG by designing the heterostructures with intrinsic electrostatic potential difference.

Physical Chemistry Chemical Physics Accepted Manuscript

One possible approach is to build the electric polarization barriers to possess a vertical built-in field between the two graphene layers by the charge-transfer interactions.[18-20] Recent studies have demonstrated that the hydrogenated BN sheets adopt sp^3-bonds between the B, N and the decorated H atoms, and thereby sustain a non-trivial bulk polarization.[18, 20] Thus, the hydrogenated BN sheets would be promising candidates to be used as polarized barriers for designing the graphene p-n vertical junctions.

In this work, we investigate a novel scheme for bipolar doping of DLG by a hydrogenated BN sandwich layer. Using the relations between the charge transfer, Fermi level shifts, and interfacial potential steps, we develop a model to predicate the Fermi level shift in the double-layer graphene as a function of the average interlayer spacing. By tuning the interlayer spacing between the graphene and hydrogenated BN as well as the thickness of BN-layered dielectric, the interfacial dipole and screening charge distribution can be modulated significantly, thereby influencing the doping level of graphene layers. This approach can be extend to incorporate other two-dimensional Janus anisotropic materials as the polarized barriers, which offer exciting opportunities for understanding two dimensional vdW heterostructures and for developing novel nanoscale electronic and optoelectronic devices.

II. Models and methods

The density function theory calculations are performed by Vienna ab initio Simulation Package (VASP) with the projector-augmented wave method.[21] In order to accurately reveal the interlayer dispersion interactions as well as the electronic structure, we have used Perdew-Burke-Ernzerhof (PBE) functional with vdW correction proposed by Grimme (DFT-D2) for generalized gradient approximation (GGA).[22, 23] The plane-wave kinetic energy cutoff, convergence criterion for energy and force were set at 500 eV, $1\text{x}10^{-7}$ eV and 0.01 eV/Å. The two-dimensional (2D)

Physical Chemistry Chemical Physics Accepted Manuscript

Brillouin zone was represented by Monkhorst-Pack special k-points of 15x15x1 for structural optimization and by 35x35x1 k-points for electronic structural calculations. To avoid interactions between layer images, a vacuum layer of 15 Å, in combination with dipole correction,[24] was adopted in the direction perpendicular to the interface.

The lateral and top views of the heterostructure are illustrated in Fig. 1. The optimized configuration of the heterostructure presents a hollow stacking, i.e., the H (hydrogen) atoms of the hydrogenated BN (HNBH: down plane N-end surface, up plane B-end surface) is located in graphene hexagonal ring center. With a commensurate stacking, the optimized planar lattice constant is 2.49 Å, which indicates 1.2% strain for graphene (the optimized lattice constant: 2.46 Å) and 3.4% compression for HNBH (the optimized lattice constant: 2.58 Å). Though the HNBH is laterally compressed, the vertical atomic positions are much less affected. The intra-layer spacing of HNBH (1.2, 0.53, 1.03 Å for H-B, B-N, N-H intra-layer, respectively) is in good agreement with the previous calculations.[20, 25] As shown in Fig. 1, the optimized equilibrium interlayer distances suggest that the space between Gr(N) (viz. graphene on the N-end surface) and HNBH (2.34 Å) is 0.12 Å shorter than that between Gr(B) (viz. graphene on B-end surface) and HNBH (2.46 Å).

III. Results and discussion

a) The electronic properties of DLG heterostructure with hydrogenated BN

To explore the DLG electronic properties, the plane averaged electrostatic potential energy is plotted. As shown in Fig. 2a, the potential energy difference

Physical Chemistry Chemical Physics Accepted Manuscript

between the two graphene layers is 1.55 eV. The imbedded potential difference breaks the interlayer symmetry, resulting in a bipolar doping of the DLG.[7, 26] This intrinsic bipolar doping of DLG is different from the graphene/BN/graphene heterostructures,[8] which doesn't need an external electric field across the layers. shown in Fig. 2b, the carbon-projected bands have broken the interlayer degeneracy. The 2p_z (circle) and 2p_y (rhombus) bands of Gr(N) (red and orange) is about 1.63 eV lower than the corresponding ones of the Gr(B) (blue and green). Two X-shaped Dirac spectrums cross at 0.83 eV (Dirac point of the Gr(B)) and -0.8 eV (Dirac point of the Gr(N)) relative to the Fermi level, which interpenetrate two Dirac cones at the Fermi surface to form a circle (see Fig. S1 in the ESI†).[26, 27] This Dirac band energy spectrum is similar to the AB type stacking bilayer graphene under a vertical field with large interlayer spacing.[27, 28] When the interlayer space larger than 5 Å, the interlayer hopping is significantly reduced and the linear band dispersion remains unchanged because of the invalid tight-binding description of Ã-B dimer state.[28] At the Γ point, the wave function of the valance band maximal (VBM) is localized on the N atoms, while the conduction band minimal (CBM) consists of near free electron (NFE) states extending into the vacuum region (Fig. 2c).[20, 29, 30] The calculated effective mass of the NFE states along the Γ-M direction 0.906 m_0 (m_0 is the mass of free electrons), which is slight smaller than that of reported NFE in h-BN multilayers (1.004 m_0).[29] This states can be attributed to the screening of surface bound charges through the short-range exchange and

Physical Chemistry Chemical Physics Accepted Manuscript

correlation and long-range Coulomb interactions, which is widely distributed in the layered compounds with Rydberg-like surfaces states, such as graphite intercalation compounds, hexagonal BN and BN multi-wall nanotubes.[20, 29, 30]

To clearly visualize the charge-transfer screening of imbedded polarized field in DLG, the charge density difference, $\Delta\rho = \rho_{\text{Gr-HNBH-Gr}} - \rho_{\text{HNBH}} - \rho_{\text{Gr-Gr}}$ is calculated (in Fig. 2d), where $\rho_{\text{Gr-HNBH-Gr}}$, ρ_{HNBH}, and $\rho_{\text{Gr-Gr}}$ are the total charge of hybrid systems, hydrogenated BN, and separated bilayer graphene, respectively. The plane averaged screening charge density along the direction perpendicular to the interface $\Delta\rho(\text{z})$ is plotted as a red line. As expected, electrons are depleted at the N-end surface and accumulated at the B-end surface. Correspondingly, the two graphene layers are doped with electrons and holes. The integration of charge density, using the well-known Poisson equation[31]

$$\nabla^2 V(\text{z}) = -e\Delta\rho(\text{z}) / A\varepsilon_0 \qquad (1)$$

where A is the area of the unit cell, e is the element charge, issues in a induced screening field $E_\rho(\text{z}) = -\nabla V(\text{z})$ (blue dotted curve in Fig. 2d). The result is shown that the maximal screening field at interface near Gr(B) is 0.35 V/Å higher than that near Gr(N), which suggests that a larger dipole induced by charge transfer between the Gr(B) and B-end surface.

b) Tuning electronic properties of DLG via the interlayer spacing

In order to further understand the different interfacial dipole on the two graphene layers, a detailed analysis of interlayer distance dependence of charge rearrangement is further performed. As shown in the inset of Fig. 3a, the plane averaged charge density differences of the DLG with different interlayer expansions are plotted. To

Physical Chemistry Chemical Physics Accepted Manuscript

quantitative study of the screening charge ($\pm\Delta\mathrm{q}$) that is responsible for the dipole on each graphene, we integrate the induced charge from the node at $z_{\mathrm{N(B)}}$ between the graphene and hydrogenated BN to the vacuum where the $\Delta\rho$ vanishes, [11, 30]

$$\pm\Delta\mathrm{q} = \int_{z_{\mathrm{N(B)}}}^{\pm\infty} \Delta\rho dz \tag{2}$$

As shown in Fig. 3a, the amount of charge depletion on the Gr(B) (i.e. $-\Delta\mathrm{q}$) is gradually diminished with enlarged interlayer spaces, while the charge accumulation on the Gr(N) (i.e., $\Delta\mathrm{q}$) firstly increases to 0.022 e and then decreases to 0.018 e. As in Fig. 3b, the corresponding screening fields $E_{\rho}(\mathrm{z})$ show the similar variation trends. This can be readily understood that the Gr(N) at the equilibrium position is associated with a "pillow effect" or "cushion effect", which drives Gr(N) to push back the electrons on the N-end surface due to the Pauli exclusion repulsion.[32-35] With small interlayer spacing, the highly overlapped charge density corresponds to enhance the Pauli repulsion on Gr(N). While for the large interlayer separation, the "pillow effect" would vanish and the interfacial dipole is exclusively contributed by charge transfer.[35] Therefore, when the layer spacing between the two graphene layers is expanded by 2Å (i.e., $Z\text{-}Z_{\mathrm{equ}}$ = d5) from its optimized positions, the transferred charges ($|\Delta\mathrm{q}|$) on both graphene layers are almost equal.

Our above results suggest that, the doping level of the DLG can be modulated by changing the interlayer spacing (i.e. interplanar strain), [27, 28] Sensitive response of DLG on the interplanar strain makes it a promising candidate for the future mechanical-electric device. Both the charge accumulation and depletion of the vdW heterostructures locate at the interface to form a separation-dependent dipole, which influences the interfacial tunnel barrier and band alignment.[33, 34, 36, 37] As shown in Fig. 4a, the alignments of valance band offsets (VBOs) and conduction band offsets

Physical Chemistry Chemical Physics Accepted Manuscript

(CBOs) for hydrogenated BN are listed with different interplanar strains on the graphene layers. The band gap of hydrogenated BN is gradually reduced with increasing the interlayer separation, which is mainly attributed to the diminished screening effects in graphene layers (Fig. 3b).[27, 28] Consequently, the reduced charge-transfer screening in graphene recovers the large spontaneous field in the hydrogenated BN, resulting in the potential energy increase on B-end surface while decrease on N-end surface. It should be noted that the NFE state wavefunction at CBM is more easily affected by the screening field than the localized wavefunction at VBM.[20, 29] As a consequence, the CBOs have a larger downward shift than the VBOs with decreasing screening field (Fig. 4a). Meanwhile, the potential difference between the two graphene layers is reduced (see Fig. S2 in the ESI†), and thereby the Dirac point shifts ($\left|E_\mathrm{D}-E_\mathrm{F}\right|=\left|\Delta E_\mathrm{F}\right|$) become smaller. It should be noted that, under the ideal conditions, the Dirac point energy levels are linearly related to the work function changes:

$$E_{\mathrm{D(n(p))}}-E_\mathrm{F}=W_{\mathrm{Gr/n(p)}}-W_{\mathrm{Gr}} \qquad (3)$$

where $W_{\mathrm{Gr/n(p)}}$ and W_{Gr} are the work function of the doped graphene and freestanding graphene, respectively.[10, 15, 26, 38] The calculated Dirac point shifts with respect to $W_{\mathrm{Gr/n(p)}}$ are plotted in Fig. 4b. The calculated work function W_{Gr} is 4.3 eV, which is slightly lower than the experimental value (4.6 eV).[10] We note that $W_{\mathrm{Gr/n(p)}}$ are higher than the values from the above linear relations when interlayer expansions are less than 1.2 Å. This indicates that $W_{\mathrm{Gr/n(p)}}$ was increased due to other dipole contributions, such as the surface dipoles and chemical interactions.[33, 35]

To further elucidate the underlying physical mechanism, the electrostatic doping of DLG can be modelled as two parallel plate capacitors, which has been successfully used to describe the Fermi level shift of graphene with metal contacts.[15] Though many

Physical Chemistry Chemical Physics Accepted Manuscript

previous calculations have focused on the single side doping graphene by stacking on various two dimensional materials substrates[16, 36, 39] (e.g., hexagonal BN and hydrogenated/fluorinated graphene), the doping mechanisms of those interfaces are different from our bipolar doping case. It should be noted that the doping levels of single layer graphene stacking on both sides of hydrogenated BN (see Fig. S3 in the ESI†) are appreciably lower than that of DLG. This indicates that the bipolar doping is mutual enhanced by the balance of screening charges between the two graphene layers, i.e., the polar charge on the B-end surface should be kept equal but opposite in sign to the charge on N-end surface.[29, 31] Therefore, the reduction of positive polar charge on B-end surface by transfer electrons from Gr(B) synergistically diminishes the negative polar charge on N-end surface by transfer electrons to Gr(N). Under the ideal conditions, the amount of transferred charge is almost equal, which results in the same magnitude but opposite direction in shifts of Fermi level in the graphene layers (i.e., the p-type doping of Gr(B) is coupled with the n-type doping of Gr(N) by the relationship: $\Delta E_{\mathrm{F(p)}} = -\Delta E_{\mathrm{F(n)}}$). As illustrated in Fig. 5, the corresponding electrostatic potential profile have the relation:

$$\Delta V = \Delta V_{\mathrm{di}} - \Delta V_{\mathrm{di(n)}} - \Delta V_{\mathrm{di(p)}} \tag{4}$$

where $\Delta V_{\mathrm{di(n(p))}}$ are the potential step terms between the graphene and the hydrogenated BN. Using the relations between the transferred charges and the Fermi level shifts, [15] we can approximated the $\Delta E_{\mathrm{F(n(p))}}$ as (see the ESI† S2):

$$\Delta E_{\mathrm{F(n(p))}} = \mp 2 \frac{\sqrt{1 + \frac{\alpha D_0}{2}(d_{\mathrm{n}} + d_{\mathrm{p}})\left|\Delta V_{\mathrm{di}} + \Delta_{\mathrm{ch}}\right|} - 1}{\alpha D_0 (d_{\mathrm{n}} + d_{\mathrm{p}})} \quad . \tag{5}$$

Here $\alpha = e^2 / \varepsilon_0 A$ is 33.88 eV/Å with A = 5.37 Å^2 the area of the unit cell, and $D_0 = D(E)/\left|E\right| \approx 0.08$ per (eV^2 unit cell) is the slop of the linear density of states for

Physical Chemistry Chemical Physics Accepted Manuscript

$|E|$ within 0.85 eV, $d_{\mathrm{n(p)}}$ are the interlayer distances between the graphene and the hydrogenated BN. When the graphene layers with large interlayer spacings, this model is in agreement with the DFT caculations (see Fig. 5b), because the chemical contribution Δ_{ch} is insignificant and the two Dirac points $E_{D(\mathrm{n(p)})}$ are distributed symmetrically bellow and above the Fermi level, respectively. We further confirm this coupled bipolar doping model by calculating the Fermi level shifts in two graphene layers with unequal expansions. As shown in Fig. S4 in the ESI†, though interlayer distances between Gr(N) and HNBH are fixed (d_n = 3.94 Å) while distances between Gr(B) and HNBH are gradually increased (d_p = $2.46+0.4x$, x= 0-5), the Fermi level shifts $\Delta E_{\mathrm{Fn(p)}}$ still agree well with the model predictions.

c) The electronic properties of DLG heterostructure with multi-layer hydrogenated cubic BN

Besides tuning the interlayer spacing, the properties of DLG can also be modified significantly by adjusting the dielectric thickness.[18, 20, 29] The multi-layer hydrogenated cubic BN (sphalerite structure) sheets exhibit labile band edge states and giant spontaneous polarization, resulting in thickness dependent metal-insulator transition.[18, 20] Here, two kinds of hydrogenated cubic BN-layered structures are considered to explore the doping properties, namely the (double-layered) Gr-H(NB)$_2$H-Gr, and (triple-layered) Gr-H(NB)$_3$H-Gr. The calculated band structures are shown in Fig. 6(a-b). Note that both Fermi levels are determined by the 2p$_x$ and 2p$_y$ hybrid states of subsurface N atoms at the B-end surface, which is different from the Fermi level settled by graphene 2p$_z$ bands in Gr-HNBH-Gr (Fig. 2b). This feature can be illustrated by the orbital-projected bands in Fig. 6(a-b). In BN-layered dielectrics, the rising 2p$_y$ band of N atoms on B-end surface pushes up the valance-band-edge states above the highest occupied level of graphene, which causes electron-hole asymmetric in the two graphene layers. Especially for the

Physical Chemistry Chemical Physics Accepted Manuscript

Gr-H(NB)$_3$H-Gr, the Dirac point shift ($\left|E_{\mathrm{D(n)}}\right| = 1.34\mathrm{eV}$) of Gr(N) is 0.5 eV larger than that ($\left|E_{\mathrm{D(p)}}\right| = 0.84\mathrm{eV}$) of Gr(B).

To further illustrate those features, we have compared the charge density differences of the DLG with different BN layers (see Fig. 6c). In Gr-H(NB)$_3$H-Gr, the "pillow effect" becomes more apparent on Gr(N).[32] A substantial charge depletes from Gr(N) and accumulates between the Gr(N) and N-end surface to form the interfacial dipole. Such a tremendous interfacial dipole contributes to the polarization and dispersion interactions for vdW adsorption.[32, 35] Indeed, according to Bader analysis, the charge transfer to Gr(N) in is 0.087 e/cell, which is larger than that in Gr-H(NB)$_2$H-Gr (0.062 e/cell), and in Gr-HNBH-Gr (0.037 e/cell). This transferred charges are qualitatively in accord with the Dirac point shifts in Gr(N). Therefore, the charge rearrangement is still dominated by charge transfer, though the "pillow effect" become more obvious.[35] A close examination of the optimized interlayer space between Gr(N) and H(NB)$_3$H is shown that the separation is 2.17 Å, which is 0.08 and 0.17 Å narrower than that for Gr-H(NB)$_2$H-Gr (2.25 Å) and for Gr-HNBH-Gr (2.34 Å), respectively. In contrast, the separations between Gr(B) and BN-layered dielectrics in their optimized structures are nearly unchanged with the increasing BN layers. It is likely that overlapping between a large amount of electrons from N-end surface and the delocalized electrons on Gr(N) in such a narrow space makes Gr(N) highly n-type doped. Thus, the remaining charge from N-end surface is not completely pushed back by the "pillow effect", which is assigned to the Gr(N) in Bader analysis.[33, 35]

From the viewpoint of potential variations (see Fig. 6d), it is shown that a potential drop induced by the spontaneous polarization in BN-layered dielectric, which influences the potential barriers at the interface and the energy levels of graphene. In comparison to Gr-HNBH-Gr, the potential barrier in Gr-H(NB)$_3$H-Gr slightly

Physical Chemistry Chemical Physics Accepted Manuscript

increases by 0.35 eV at the B-end surface, while the one at the N-end surface drops by 2 eV. This larger potential drop on N-end surface would affect the energy bands in Gr(N). In general, the shift of graphene bands are contributed by the two electrostatic potentials, namely, the surface potential and the Hartree potential of the charge density difference.[35] Especially for small adsorption distance, both potentials have a large impact on the energy level of the adsorbate by the Coulomb and exchange-correlation interactions.[33, 35] Therefore, the decreased surface potential on N-end surface combined with the Hartree potential induced by charge transfer can lower the Gr(N) bands significantly.

Furthermore, the $2p_y$ bands of N atom in different BN layers reflect the potential changes between the dielectrics. As shown in Fig. 6(a-b), the N atom $2p_y$ band shift in Gr-H(NB)$_2$H-Gr is obviously larger than that in Gr-H(NB)$_3$H-Gr. This indicates that the polarized field decreases with increasing the layer of BN dielectrics. Generally, when the potential drop is less than the band gap, the polarized field in nitrides quantum well is uniform: $\left|\vec{E}\right| = 4\pi \vec{P} / \varepsilon$, and the potential drop grows linearly with the thickness.[40] As the potential drop is close to the band gap, the Fermi level approaches the conduction band edge, which generates free carriers to neutralize part of the effective polarization charges and thereby reduces the polarized field with increasing thickness.[19, 40] In the present case, the charge carriers in graphene layers can play the same role for the neutralization, causing the built-in polarization field decrease in the thick BN-layered dielectrics.[31]

d) Prospects

From the above discussions, we would like to mention that the proposed bipolar doping DLG strategy can extend to other two-dimensional Janus anisotropic materials, such as hydro-fluorinated carbon or boron nitride-based nanofilms.[16, 18, 19, 25] The H and F atoms co-decorated on two sides of pristine BN or carbon films break the inversion symmetry and possess a spontaneous polarization. It is convenient to

Physical Chemistry Chemical Physics Accepted Manuscript

Physical Chemistry Chemical Physics Accepted Manuscript

dope the DLG with wide range of carrier density using these Janus anisotropic materials by adjusting the F atom concentrations (see Fig. S5 in the ESI†). Additionally, using the Gr-FCCH-Gr as the sandwich layer, the graphene Fermi level shifts as a function of the average interlayer distances are still agree with the model predictions (see Fig. S6 in the ESI†). Previously experiments have successfully functionalized the BN or carbon films with H and F atoms by chemical treatment.[41-43] These highly controllable doping level of graphene vertical p-n junctions would be useful for carbon-based diode applications.[4, 8, 13] Compared with the most graphene heterostructures spatially selective doping with two types of dopants or asymmetric metal electrodes,[3-5, 13, 44] bipolar doping the DLG by two-dimensional Janus materials is a concept worthy of attention, because the doped graphene layers are mutually coupled and their Dirac electron properties are still preserved. The vertical internal field existed between the graphene heterostructure is responsible for separation of photo-generated electron-hole pairs,[9, 14, 45] which is the key process for graphene broadband photodetection. Because very short lifetime of the photoexcited carriers requires separated efficiently in sub-picosecond timescale to generate a photocurrent.[9, 14, 46] The DLG heterostructures have large detection areas for the vertical stacking, which makes striking superiority for photocurrent extraction. Furthermore, many new physical questions emerge from such atomically thin p-n junctions, like exciton condensation and Coulomb coupling between the adjacent layers,[1, 2, 7, 14] which offers exciting opportunities for understanding two dimensional vdW heterostructures and for developing novel atomic-scale optoelectronic and mechanical-electric devices.

IV. Conclusions

In summary, we propose a scheme for bipolar doping DLG heterostructures by a hydrogenated BN sandwich layer. First-principles calculations indicate that a spontaneous polarized field in hydrogenated BN sheets breaks the symmetry between the graphene layers, resulting in a bipolar doping of the DLG. By tuning the interlayer spacing between the graphene and hydrogenated BN, the coupled charge redistributions and band offsets of the DLG can be modulated gradually. Using the relations between the charge transfer, Fermi level shifts, and interfacial potential steps, we have developed an analytical model to describe the graphene Fermi level shift as a function of the average interlayer spacing. Moreover, with increased the BN dielectric layers, the rising $2p_y$ band of N atoms on B-end surface pushes up the valance-band-edge states above the highest occupied level in graphene, which causes electron-hole asymmetric in the two graphene layers. This bipolar doping of DLG by two-dimensional Janus materials is a concept worthy of attention, which may be important to the development of novel optoelectronic and electronic devices.

Acknowledgements

The work was financially supported by National Natural Science Foundation of China (NSFC) (Grant Nos. 51472010 and 11274029), the Importation and Development of High-Caliber Talents Project of Beijing Municipal Institutions (No.CIT&TCD201204037), the Jing-Hua Talents Project of Beijing University of Technology (No. 2014-JH-L07) and the Foundation on the Creative Research Team Construction Promotion Project of Beijing Municipal Institution (No. IDHT20140506).

Footnote

† Electronic supplementary information (ESI) available: Calculated Dirac band energy spectrum (above the Fermi level part) of DLG; plane averaged potential

Physical Chemistry Chemical Physics Accepted Manuscript

energies of DLG with the expanded interlayer distances; band structures of single layer graphene adsorption on HNBH; the Fermi level shifts versus the averaged interlayer distances in two graphene layers with unequal expansions; using hydrofluorinated graphene Gr-(F_xH_{1-x})CCH-Gr as the sandwich layer, the DLG with controllable doping level by adjusting the F atom concentrations; using the hydro-fluorinated graphene Gr-FCCH-Gr as the sandwich layer, the graphene Fermi level shifts versus the average interlayer distances; and the electrostatic doping model for double-layer graphene heterostructure (in the S2) are collected.

References

1. P. Avouris, *Nano Lett.*, 2010, **10**, 4285.
2. A. H. Castro Neto, N. M. R. Peres, K. S. Novoselov and A. K. Geim, *Rev. Mod. Phys.*, 2009, **81**, 109.
3. V. V. Cheianov, V. Fal'ko and B. L. Altshuler, *Science*, 2007, **315**, 1252.
4. T. Mueller, F. Xia and P. Avouris, *Nat. Photonics*, 2010, **4**, 297.
5. Y. Xue, B. Wu, Q. Bao and Y. Liu, *Small*, 2014, **10**, 2975.
6. F. Schwierz, *Nat. Nanotechnol.*, 2010, **5**, 487.
7. R. V. Gorbachev, A. K. Geim, M. I. Katsnelson, K. S. Novoselov, T. Tudorovskiy, I. V. Grigorieva, A. H. MacDonald, S. V. Morozov, K. Watanabe, T. Taniguchi and L. A. Ponomarenko, *Nat. Phys.*, 2012, **8**, 896.
8. L. Britnell, R. V. Gorbachev, R. Jalil, B. D. Belle, F. Schedin, A. Mishchenko, T. Georgiou, M. I. Katsnelson, L. Eaves, S. V. Morozov, N. M. Peres, J. Leist, A. K. Geim, K. S. Novoselov and L. A. Ponomarenko, *Science*, 2012, **335**, 947.
9. L. Britnell, R. M. Ribeiro, A. Eckmann, R. Jalil, B. D. Belle, A. Mishchenko, Y.-J. Kim, R. V. Gorbachev, T. Georgiou, S. V. Morozov, A. N. Grigorenko, A. K. Geim, C. Casiraghi, A. H. C. Neto and K. S. Novoselov, *Science*, 2013, **340**, 1311.

Physical Chemistry Chemical Physics Accepted Manuscript

10. Y.-J. Yu, Y. Zhao, S. Ryu, L. E. Brus, K. S. Kim and P. Kim, *Nano Lett.*, 2009, **9**, 3430.

11. W. Zhu, H. Chen, K. H. Bevan and Z. Zhang, *ACS Nano*, 2011, **5**, 3707.

12. H. Wang, F. Liu, W. Fu, Z. Fang, W. Zhou and Z. Liu, *Nanoscale*, 2014, **6**, 12250.

13. S. Kim, D. H. Shin, C. O. Kim, S. S. Kang, J. M. Kim, C. W. Jang, S. S. Joo, J. S. Lee, J. H. Kim, S.-H. Choi and E. Hwang, *ACS Nano*, 2013, **7**, 5168.

14. C.-H. Lee, G.-H. Lee, A. M. van der Zande, W. Chen, Y. Li, M. Han, X. Cui, G. Arefe, C. Nuckolls, T. F. Heinz, J. Guo, J. Hone and P. Kim, *Nat. Nanotechnol.*, 2014, **9**, 676.

15. G. Giovannetti, P. Khomyakov, G. Brocks, V. Karpan, J. van den Brink and P. Kelly, *Phy. Rev. Lett.*, 2008, **101**, 026803.

16. X. Lin, Y. Xu, A. A. Hakro, T. Hasan, R. Hao, B. Zhang and H. Chen, *J. Mater. Chem. C*, 2013, **1**, 1618.

17. F. H. L. Koppens, T. Mueller, P. Avouris, A. C. Ferrari, M. S. Vitiello and M. Polini, *Nat. Nanotechnol.*, 2014, **9**, 780.

18. W. Chen, Y. Li, G. Yu, C.-Z. Li, S. B. Zhang, Z. Zhou and Z. Chen, *J. Am. Chem. Soc.*, 2010, **132**, 1699.

19. Z. Zhang, X. C. Zeng and W. Guo, *J. Am. Chem. Soc.*, 2011, **133**, 14831.

20. Z. Zhang and W. Guo, *Nano Lett.*, 2012, **12**, 3650.

21. G. Kresse and J. Furthmüller, *Phys. Rev. B*, 1996, **54**, 11169.

22. S. Grimme, *J. Comput. Chem.*, 2006, **27**, 1787.

23. J. Klimeš, D. R. Bowler and A. Michaelides, *Phys. Rev. B*, 2011, **83**, 195131.

24. G. Makov and M. C. Payne, *Phys. Rev. B*, 1995, **51**, 4014.

25. Q. Tang, J. Bao, Y. Li, Z. Zhou and Z. Chen, *Nanoscale*, 2014, **6**, 8624.

26. K. S. Kim, A. L. Walter, L. Moreschini, T. Seyller, K. Horn, E. Rotenberg and A. Bostwick, *Nat. Mater.*, 2013, **12**, 887.

27. B. Nanda and S. Satpathy, *Phys. Rev. B*, 2009, **80**, 165430.

28. Y. Guo, W. Guo and C. Chen, *Appl. Phys. Lett.*, 2008, **92**, 243101.

29. M. Otani and S. Okada, *Phys. Rev. B*, 2011, **83**, 073405.

Physical Chemistry Chemical Physics Accepted Manuscript

30. M. Feng, J. Zhao and H. Petek, *Science*, 2008, **320**, 359.

31. E. J. Santos and E. Kaxiras, *Nano Lett.*, 2013, **13**, 898.

32. T. Bauert, L. Zoppi, G. Koller, A. Garcia, K. K. Baldridge and K.-H. Ernst, *J. Phys. Chem. Lett.*, 2011, **2**, 2805.

33. O. L. A. Monti, *J. Phys. Chem. Lett.*, 2012, **3**, 2342.

34. C. Gong, L. Colombo, R. M. Wallace and K. Cho, *Nano Lett.*, 2014, **14**, 1714.

35. J. Gebhardt, F. Viñes and A. Görling, *Phys. Rev. B*, 2012, **86**, 195431.

36. Y. Xu, Y. Liu, H. Chen, X. Lin, S. Lin, B. Yu and J. Luo, *J. Mater. Chem.*, 2012, **22**, 23821.

37. Y. Ma, Y. Dai, M. Guo, C. Niu and B. Huang, *Nanoscale*, 2011, **3**, 3883.

38. S. Yang, P. Zhou, L. Chen, Q. Sun, P. Wang, S. Ding, A. Jiang and D. W. Zhang, *J. Mater. Chem. C*, 2014, **2**, 8042.

39. S. Tang, J. Yu and L. Liu, *PCCP*, 2013, **15**, 5067.

40. F. Bernardini and V. Fiorentini, *Appl. Surf. Sci.*, 2000, **166**, 23.

41. C. Tang, Y. Bando, Y. Huang, S. Yue, C. Gu, F. Xu and D. Golberg, *J. Am. Chem. Soc.*, 2005, **127**, 6552.

42. R. Stine, W.-K. Lee, K. E. Whitener, J. T. Robinson and P. E. Sheehan, *Nano Lett.*, 2013, **13**, 4311.

43. L. Liao, H. Peng and Z. Liu, *J. Am. Chem. Soc.*, 2014, **136**, 12194.

44. H. L. Poh, P. Simek, Z. Sofer, I. Tomandl and M. Pumera, *J. Mater. Chem. A*, 2013, **1**, 13146.

45. Z. Liu, R.-Z. Wang, L.-M. Liu, H. Yan and W.-M. Lau, *J. Mater. Chem. A*, 2014, **2**, 9744.

46. Z. Sun and H. Chang, *ACS Nano*, 2014, **8**, 4133.

Physical Chemistry Chemical Physics Accepted Manuscript

Figures captions:

Fig. 1. Optimized structure of DLG with a hydrogenated BN sandwich layer (optimised atomic plane positions and interlayer distances of Gr-HNBH-Gr are represented by dashed lines and numbers (distance unit: Å), respectively).

Fig. 2. (a) The plane averaged electrostatic potential energy is plotted in red line. (b) Caculated orbit-projected band structure of DLG. The contributions of graphene $2p_z$ (circle) and $2p_y$ (rhombus) orbitals to the bands are colored (Gr(N) with red and orange, and the Gr(B) with blue and green). (c) Plane averaged wavefunction square of VBM and CBM at the Γ point. (d) Plane integrated charge density difference $\Delta\rho(z)$ is plotted by red line. The blue dotted curve indicates the electric field $E_\rho(z)$ induced by the charge redistribution.

Fig. 3. (a) Amount of charge transfer between hydrogenated BN and graphene layers versus the expanded interlayer spacings ($Z\text{-}Z_{equ}$ denote the distances of graphene layers departure from their optimised equamlium positions in C axis). The red(blue) trangles are denote the electron accumlation(depletation) on Gr(N)(Gr(B)). The inset show plane integrated charge density differences with enlarged interlayer spacing ($Z\text{-}Z_{equ} = ds = 0.4\times s$ (Å), s =1-5, and d0 denotes the optimised interlayer spacing). (b) The charge-transfer screening fields varying with expanded interlayer spacings.

Physical Chemistry Chemical Physics Accepted Manuscript

Fig. 4. (a) The alignments of VBOs (valance band offsets) and CBOs (conduction band fsets) for hydrogenated BN are listed with different interplanar strains on the graphene layers. The energy regions of the two X-shaped cross Dirac spectrums are also drawn (red (yellow) for n-type (p-type) doping). (b) Calculated Dirac point shifts versus the work functions with different interlayer spacings.

Fig. 5. (a) Schematic illustration of the bipolar doping in DLG heterostructure with inserted hydrogenated boron nitride dielectrics (more details see the ESI† S2). (b) The Fermi level shifts in the graphene layers versus the average interlayer spacings. The results given by sloid lines represent the model predictions, the dots are obtained from the DFT caculations.

Fig. 6. (a-b) Band structures of DLG with multi-layer hydrogenated BN dielectrics, (double-layered) Gr-H$(NB)_2$H-Gr (a), and (triple-layered) Gr-H$(NB)_3$H-Gr (b). The dotted bands are contributed by N $2p_y$ orbitals on different layer (count from N-end to B-end surface: 1st circle, 2nd square, 3rd diamand). (c) Plane integrated charge density differences between the two graphene layers and BN-layered dielectrics. (d) Plane averaged potential energies of DLG with different BN-layered dielectrics. The potential barriers between the graphenes and BN-layered dielectrics are hightlighted by squares.

TOC figure:

Bipolar Doping of Double-layer Graphene Vertical Heterostructures with Hydrogenated Boron Nitride.

Physical Chemistry Chemical Physics Accepted Manuscript

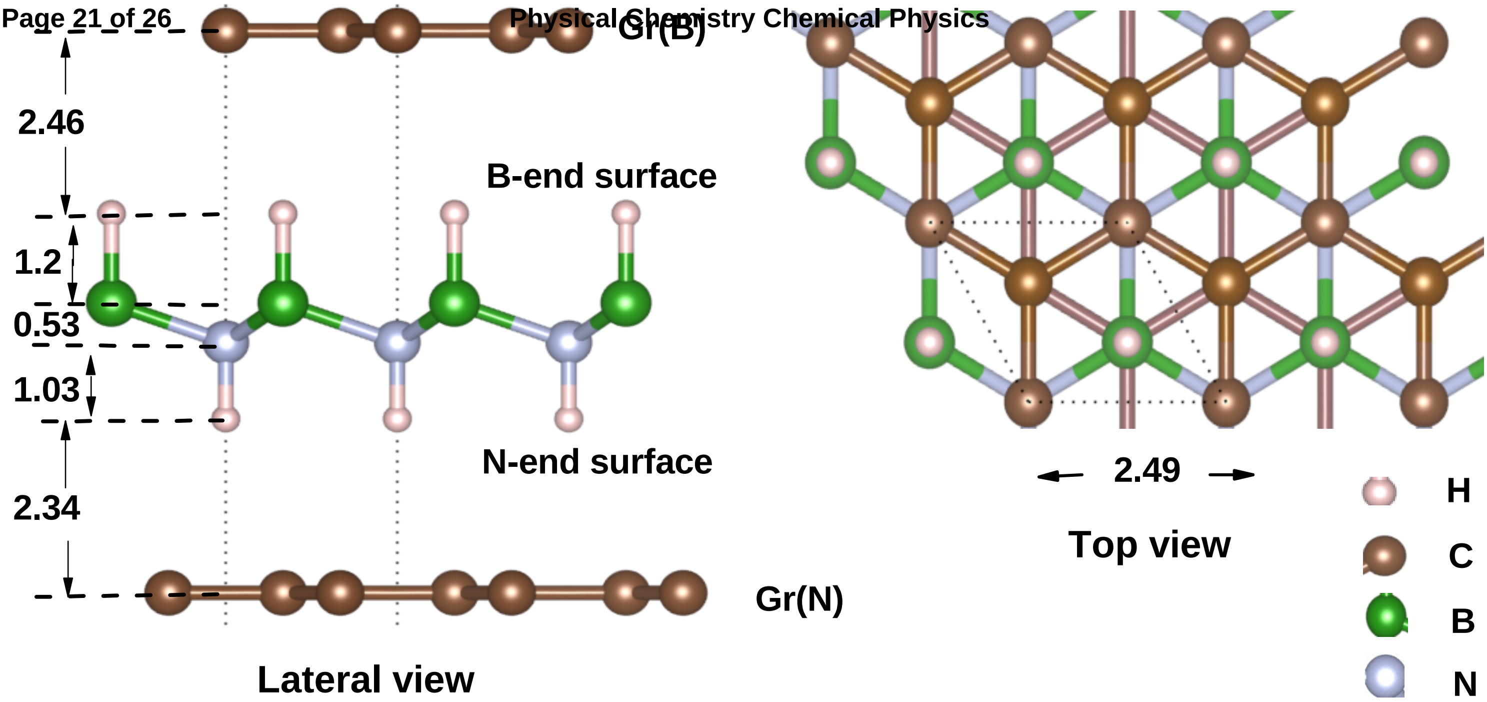

Physical Chemistry Chemical Physics Accepted Manuscript

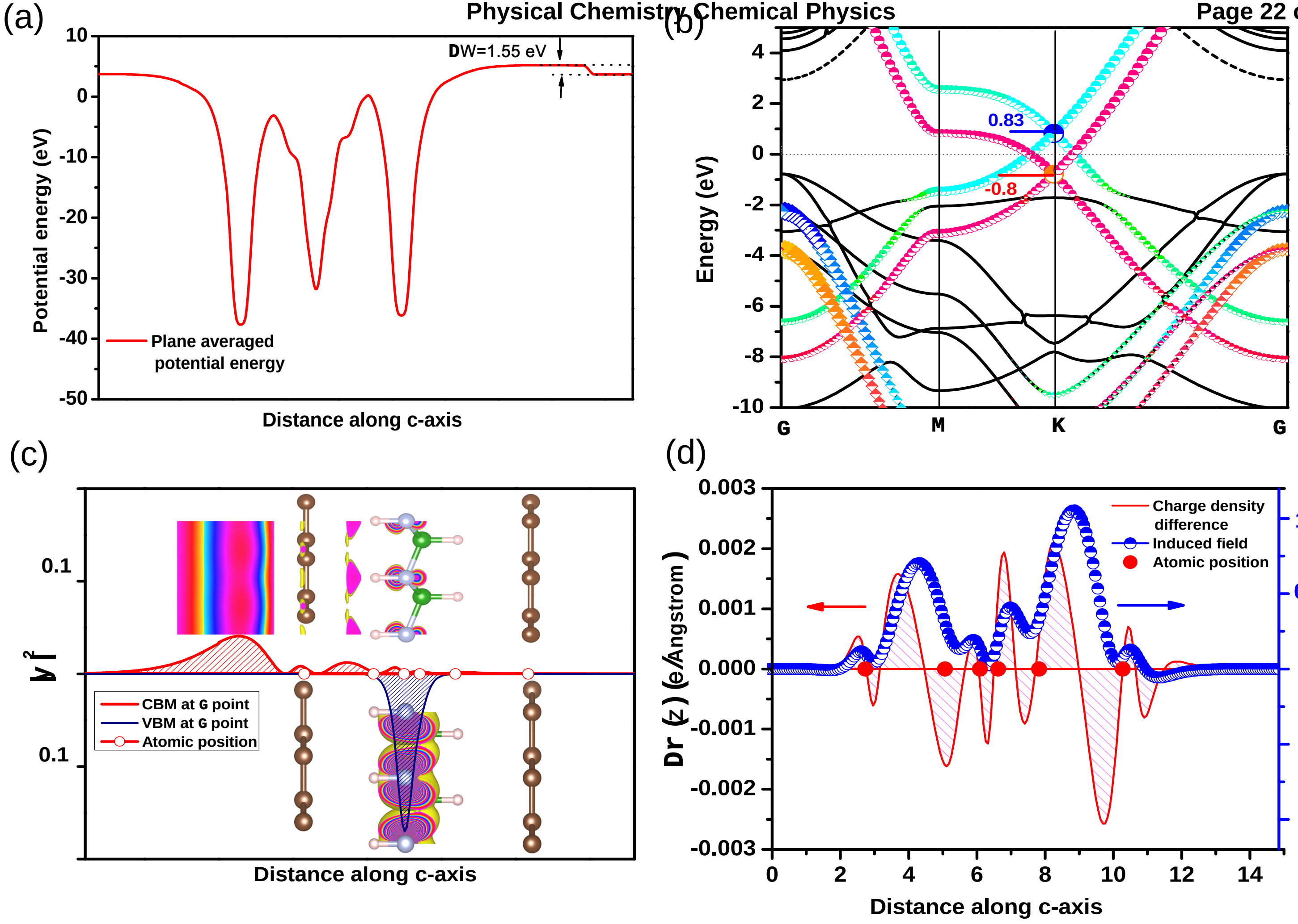

Physical Chemistry Chemical Physics Accepted Manuscript

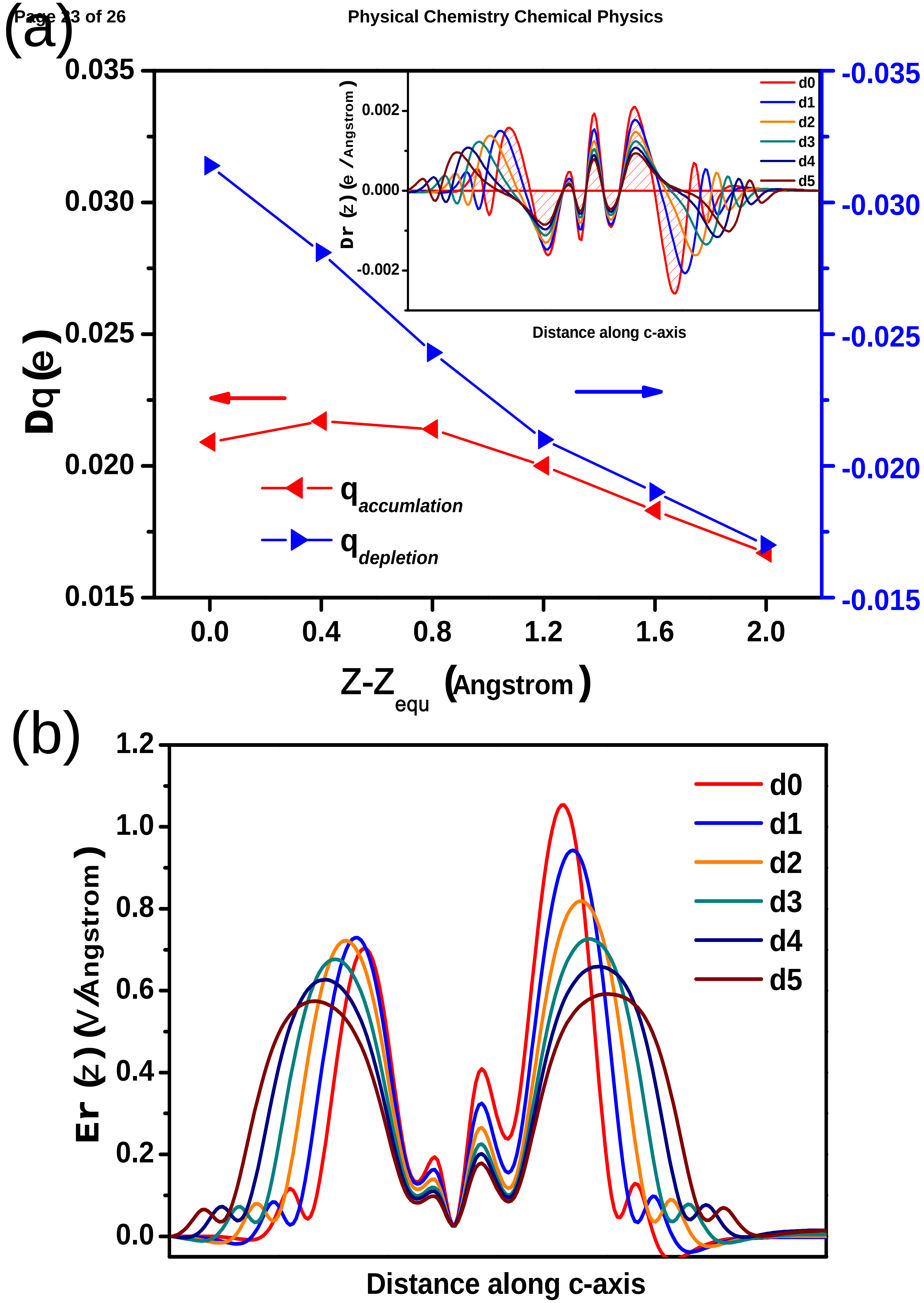

Physical Chemistry Chemical Physics Accepted Manuscript

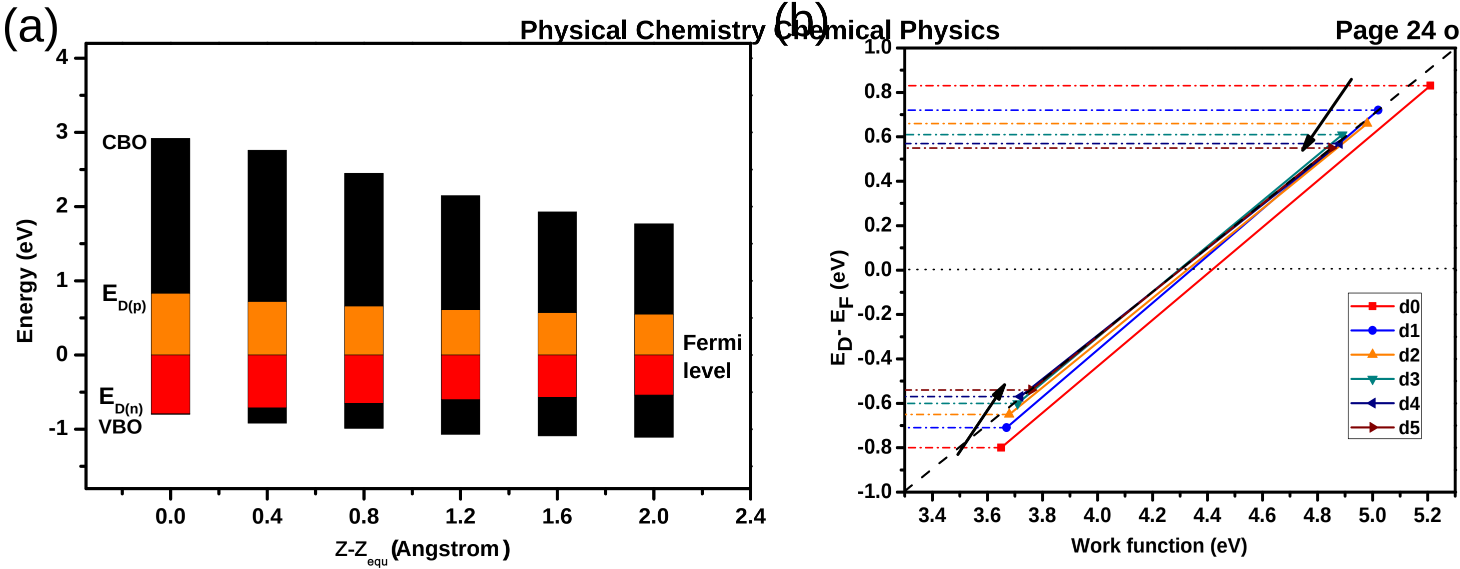

Physical Chemistry Chemical Physics Accepted Manuscript

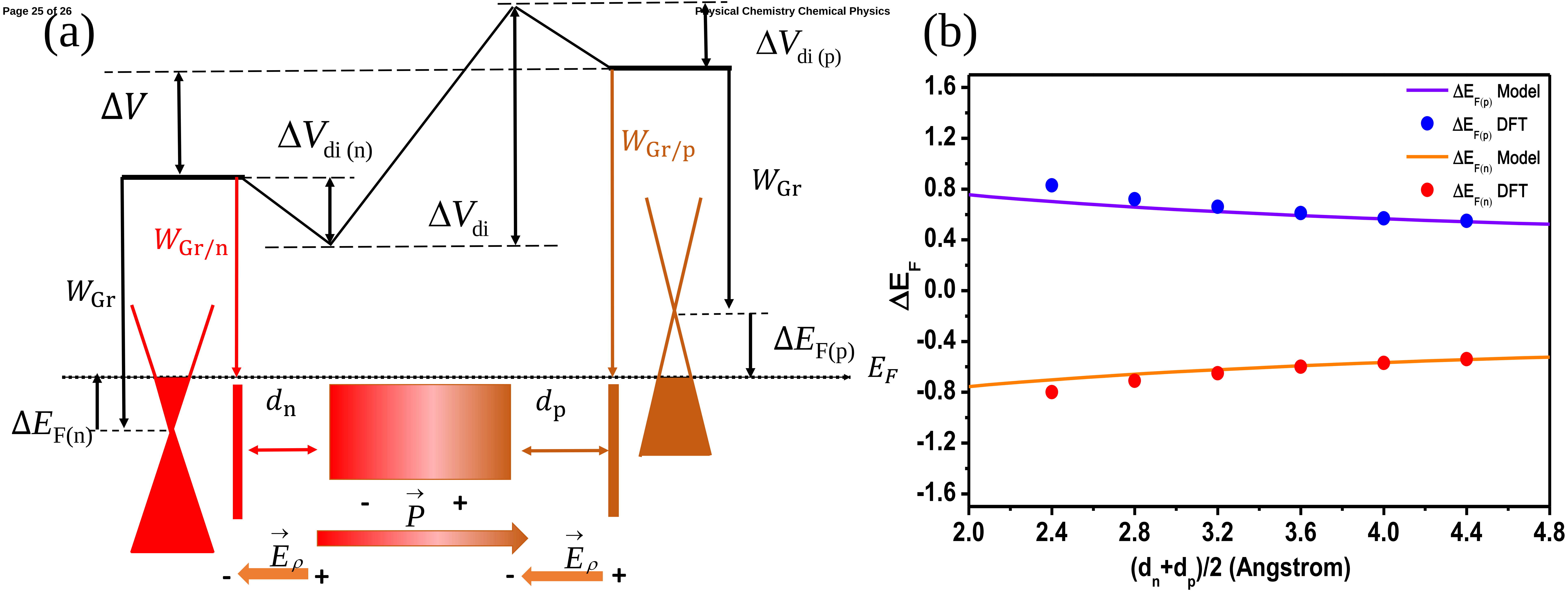

Physical Chemistry Chemical Physics Accepted Manuscript

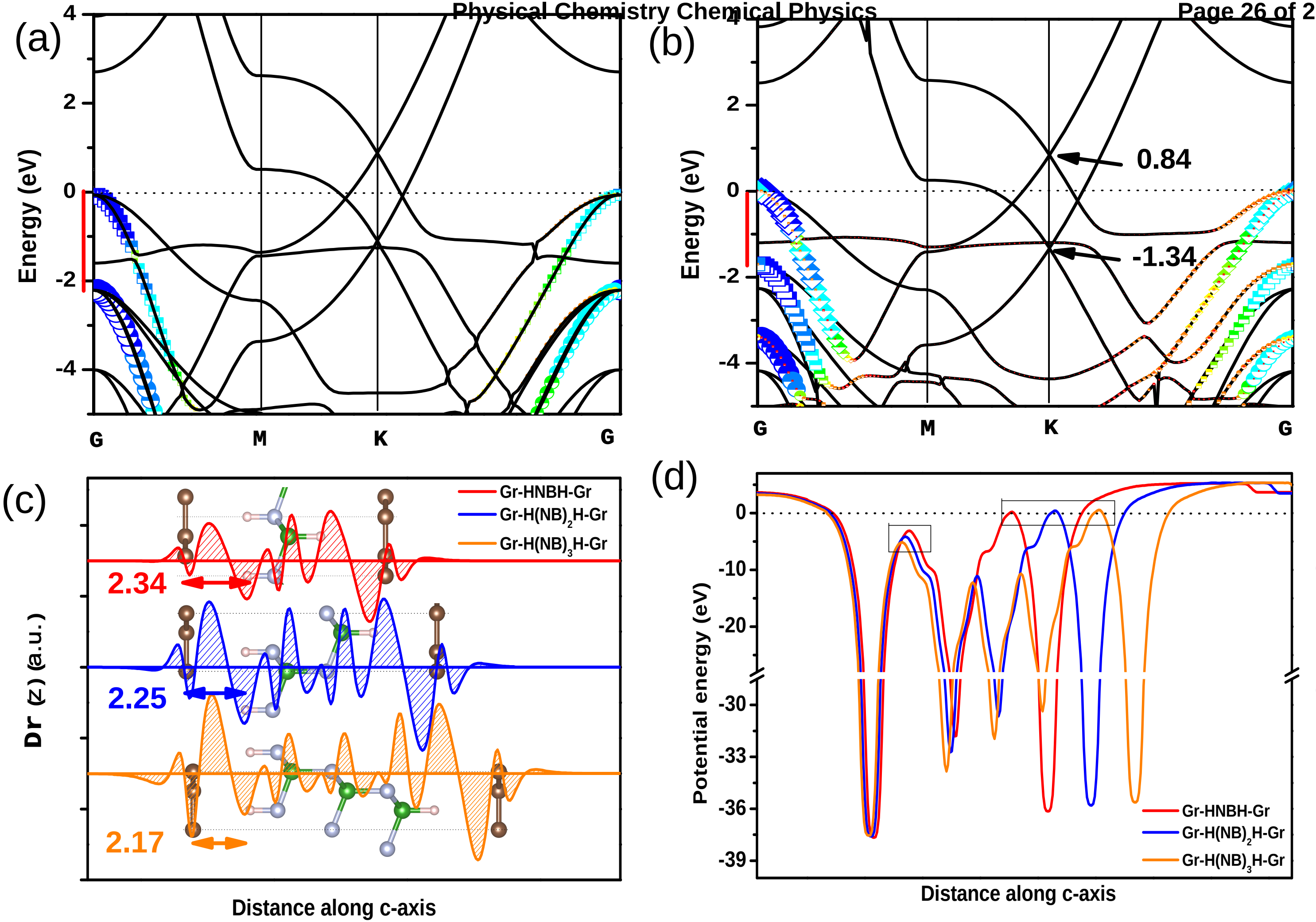

Physical Chemistry Chemical Physics Accepted Manuscript